Nanoscale

Accepted Manuscript

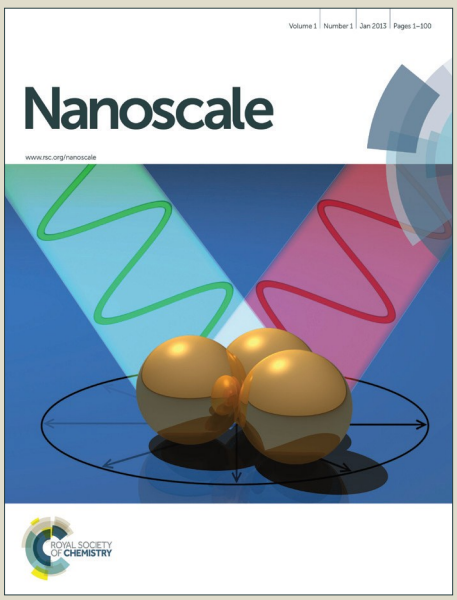

ROYAL SOCIETY OF CHEMISTRY

www.rsc.org/nanoscale

Journal Name

ARTICLE

Solvothermal Synthesis of Superhydrophobic Hollow Carbon Nanoparticles from Fluorinated Alcohol

Received 00th January 20xx,
Accepted 00th January 20xx

DOI: 10.1039/x0xx00000x

www.rsc.org/

S. M. Lyth,[*afgh] W. Ma,[a] J. Liu,[ab] T. Daio,[bc] K. Sasaki,[abcd] A. Takahara,[ae] and B. Ameduri[i]

A new and simple method of synthesizing fluorinated carbon at gram scale is presented by reacting a fluorinated alcohol with sodium at elevated temperature in a sealed Teflon reactor. The resulting carbon nanoparticles are around 100 nm in diameter, and display a hollow shell morphology, with significant fluorine doped into the carbon. The nanoparticles disperse easily in ethanol, and are thermally stable at up to 400 °C and 450 °C under air and nitrogen, respectively. The nanoparticle dispersion was printed onto various different substrates (paper, cloth, silicon), inducing superhydrophobicity.

Introduction

Fluorination has proven to be an effective method to tailor the properties of a wide range of carbon materials.[1] Graphite fluoride is the most well established covalently bonded fluorocarbon, formed by a harsh fluorination of graphite. It has several interesting properties; it is electrically insulating, thermally conductive, has low shear strength, and has a wide band gap. It is widely used as an electrode in lithium batteries,[2] as a solid lubricant, and as an additive for weather resistant paint.[3]

Fluorination of carbon-based materials such as carbon blacks;[4] carbon fibers;[5–9] single wall carbon nanotubes;[10–12] multiwall carbon nanotubes;[13–16] and graphene,[14,17–22] has been explored extensively in recent decades. There are several main methods for the preparation of fluorocarbons: direct fluorination in F_2 gas at elevated temperature, sometimes in the presence of HF or IF_5 (at 150 to 600°C);[16] radio-frequency plasma treatment in CF_4 gas;[23] chemical vapor deposition from perfluorohexane at 100 to 500˚C,[6] or chemical vapor deposition in CF_4 plasma at room temperature;[19] decomposition of xenon difluoride (XeF_2);[18] mechanical exfoliation of graphite fluoride;[24] arc discharge between graphite fluoride-containing graphite rods;[14] coating with fluorinated silane;[25] heating carbon in TbF_4;[26] reduction of graphene oxide in HF,[27] or the use of perfluoropolyether peroxide.[28] In addition, coating e.g. carbon nanotubes forests with PTFE can result in superhydrophobic "fluorinated" carbons.[29] Of these methods, direct fluorination in F_2 or XeF_2 is by far the most common.

Fluorination of nanostructured carbons generally results in modification of the electronic properties. For example, fluorinated graphene has been used as a transistor,[22] and colossal negative magnetoresistance has been observed.[21] The optical properties can also be drastically modified; fluorinated carbons can be grey, white, or even transparent due to the induced wide band-gap of around 3.8 eV.[22,30] Fluorographene has also been reported to be magnetic,[17,31] and has improved electron field emission properties.[32]

In particular, the wettability of the surfaces of materials can be modified by fluorination. Fluoropolymers have provided good control of surface wettability control, with low hysteresis and superhydrophobicity.[33–35] Due to the low surface free energy and appropriate microscopic surface roughness, fluorocarbons can also display superhydrophobic properties.[36] Superhydrophobic surfaces have very weak interaction with water, resulting in extremely high water contact angle (CA >150°) and low water sliding angle (SA < e.g. 30°).[37–42] Meanwhile, the dispersion of carbon in organic solvents can be enhanced by fluorination, thus enabling solution based applications.[43]

Superhydrophobic materials are industrially useful in such applications as e.g. self-cleaning surfaces;[44,45] fluidic drag reduction;[46,47] enhancing water supporting force in membranes; bio-surfaces; corrosion prevention; preventing snow/ice accumulation; enhancing buoyancy; flow management in microfluidic devices;[48] and oil spill cleaning.[49] In electrochemical devices such as polymer electrolyte

[a] International Institute for Carbon-Neutral Energy Research (WPI-I2CNER);
[b] Department of Mechanical Engineering;
[c] International Research Center for Hydrogen Energy;
[d] Next-Generation Fuel Cell Research Center;
[e] Institute for Materials Chemistry and Engineering; Kyushu University, 744 Motooka, Nishi-ku, 819-0395, Fukuoka, Japan
[f] School of Chemical and Process Engineering, Faculty of Engineering, University of Leeds, LS2 9JT, UK
[g] Energy Engineering Group, Department of Mechanical Engineering, University of Sheffield, S10 2TN, UK
[h] CREST, Japan Science and Technology Corporation, Kawaguchi, 332-0012, Japan
[i] Ingénierie et Architectures Macromoléculaires, Institut Charles Gerhardt UMR CNRS 5253; Ecole Nationale Supérieure de Chimie de Montpellier, 8 rue de l'Ecole Normale, 34296 Montpellier Cedex 5, France
† Corresponding author: lyth@physics.org

membrane fuel cells (PEMFCs), water electrolysis, and batteries, water management is of great importance to prevent flooding.[50] Superhydrophobic materials can be of great help in this case.

Here we present a new and simple method of synthesizing fluorinated carbon nanoparticles at gram scale by solvothermal reaction between fluorine-containing alcohol and sodium metal. The resulting carbon coating displays superhydrophobic properties.

Methods

All chemicals were used as received from suppliers, without further purification. $C_6F_{13}CH_2CH_2OH$ was synthesized according to a procedure previously reported,[51] from the ethylenation of $C_6F_{13}I$ followed by oxidation in a water / dimethylformamide (DMF) mixture. 5 mL (8.35 g) of $C_6F_{13}CH_2CH_2OH$ was directly reacted with sodium metal (2.04 g, Sigma-Aldrich) in a sealed polytetrafluoroethylene (PTFE) melting pot (Flon Industry, Japan) at 180 ˚C for 2 days, and then cooled to room temperature. White smoke was emitted when the lid was opened which may be HF formed during decomposition of the precursor. Therefore great care must be taken when performing this reaction. The PTFE in the melting pot was discolored and misshapen after the reaction, suggesting that the reaction was exothermic and reached a temperature higher than recommended for PTFE parts (~220-250 ˚C), and / or that the fluorinated precursors strongly interact with PTFE. The black, dry product was dispersed with large white lumps and white powder. This was dispersed in a 50/50 vol.% mixture of ethanol and deionized water, sonicated for 1 h, then vacuum filtered in order to remove the byproducts.

Scanning electron microscopy (SEM, S-5200, Hitachi, Japan); dark field transmission electron microscopy (TEM) coupled with EDX mapping (JEM-ARM200F, JEOL, Japan); high resolution TEM (HRTEM) with selected area electron diffraction (SAED) (Tecnai-20, Philips, at 200 kV); Brunauer–Emmett–Teller theory nitrogen adsorption surface area analysis (BET, Belsorp Mini II-VS, Bel Japan, Inc.); thermo-gravimetric analysis (TGA, TG 8120, Rigaku Corp., Japan) measured under nitrogen or air at 10 °C min^{-1}; Raman spectroscopy (DM2500M, Renishaw, UK, using an argon-ion laser at 532 nm); X-ray diffraction (XRD, RINI Ultima III, Rigaku, Japan, Cu Kα-radiation, λ = 1.54 Å); X-ray photoelectron spectroscopy (XPS, ESCA-3400, Kratos Analytical Ltd., UK); and contact angle measurements (Attension Theta system, KSV Instruments Ltd., equipped with a CCD camera), were used to characterize the material.

Results and Discussion

Reaction Description

The as-synthesized product was a highly flocculent dry black powder. The white byproducts were confirmed to be sodium fluoride and sodium oxides by XPS. After drying under vacuum, the final product mass was 1.75 g, corresponding to a yield of 20 wt%. A non-stoichiometric reaction scheme detailing the probable products of the decomposition is presented below:

$$C_6F_{13}\,CH_2CH_2OH + Na \xrightarrow{180^o,\ decomposes} CF_x + H_2 + HF + NaF + NaO(H) \qquad (1)$$

We have previously performed similar experiments reacting sodium with simple hydrogenated alcohol (ethanol/ diethanolamine).[52–54] In those cases, sodium alkoxide powders were formed, and the material did not directly decompose into carbon. Those products were burned in air and decomposed to form defective graphene, and nitrogen-doped graphene macroporous open-cell foams, with a similar yield of around 15 wt%.

Electron Microscopy

SEM (Figure 1a) reveals that the product is comprised of interconnected spheroidal nanoparticles with a diameter of 50 to 100 nm. These nanoparticles cluster together, and are interspersed with micron-scale voids. This structure is highly uniform over a large scale and these images are representative of the whole sample, with the exception of a few clusters of much larger spheroidal particles up to around 1 µm in diameter. The nanoparticles are highly reminiscent of the structure of carbon black (e.g. Vulcan XC-72, *Cabot Corporation, US*, Figure 1b), although with a slightly larger particle size. In the case that ethanol is used in place of the fluorinated alcohol, a completely different structure is produced after decomposition; an open-cell defective graphene foam, as explored extensively in our previous studies.[52–54] TEM images (Figure 1c-f) immediately reveal that most of these nanoparticles have a hollow shell morphology, and a few are solid. The thickness of the shell walls is around 10 nm, and there is a relatively electron dense spheroid located inside many of them.

Elemental Mapping

EDX elemental analysis on the region shown in Figure 1d gives a carbon content of 94.9 at.%, a fluorine content of 2.63 at.%, and a sodium content of 2.43 at.%. EDX elemental mapping (Figure. 1g-i) suggests that the material inside the shell is sodium fluoride, whilst the shell itself comprised carbon and fluorine. Selective elemental mapping of the dense inner material reveals approximately equal proportions of Na (5.76 at.%) and F (5.21 at.%), confirming the presence of NaF. Selective elemental analysis of only the shell region (avoiding the NaF particle in the center) gives a carbon content of 96.64 at.%, a fluorine content of 2.39 at.%, and a sodium content of 0.97 at.%. This difference confirms that fluorine is doped into the walls of the nanoparticles. In comparison, unfluorinated carbon derived from ethanol and sodium is measured to have a carbon content of 96.4 at.% and an oxygen content of 3.6 at.%.

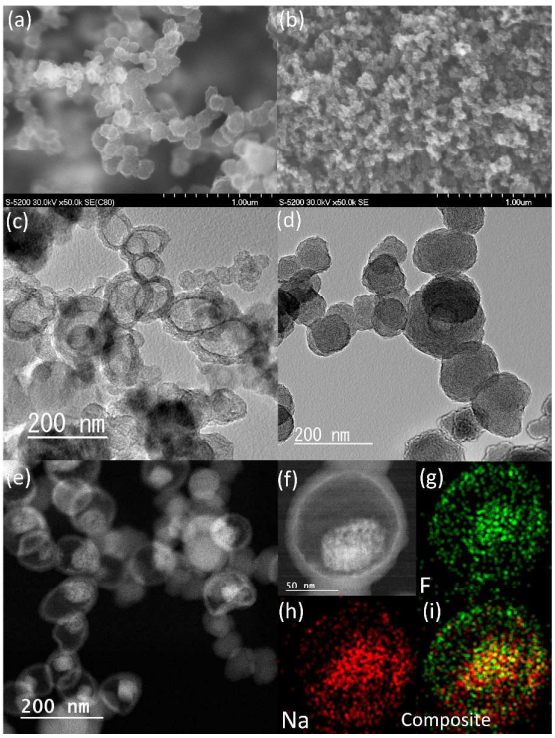

Fig. 1 SEM images of (a) fluorinated carbon nanoparticles and (b) carbon black. TEM images (c-e) of the fluorinated carbon nanoparticles. EDX elemental analysis of the fluorinated carbon nanoparticles: elemental mapping of (g) F and (h) Na. (i) Corresponding composite map.

X-ray Photoelectron Spectroscopy

Several XPS studies have been carried out on fluorocarbons indicating several main bonding types. Mild fluorination or intercalation results in weak semi-ionic bonding, whereas harsher processing (e.g. at higher temperature) results in a greater degree of covalent bonding.[4,11,15,55] The C1s spectra of fluorinated carbons are generally deconvoluted into separate peaks corresponding to CF (~ 289.6 eV), CF_2 (~ 291.5 eV) and CF_3 (~ 294.0 eV), and semi-ionic bonds (~ 286.4 eV), as well as sp^2 carbon at 284.5 eV and carbon-oxygen bonds at ~ 285.5 eV. F 1s spectra are not reported to show such distinct regions and are generally only deconvoluted into covalent (~ 688.3 eV), semi-ionic (~ 686.5 eV), and ionic (~ 684 eV) bonds. All of these peak assignments depend somewhat upon the structure of the carbon skeleton. Additionally, due to the electrical resistivity of fluorinated carbons, some charging effects are also expected, shifting the spectra in the positive binding energy direction.

The XPS wide-scan for the nanoparticles synthesized in this work is shown in Figure 2a. High resolution scans (Figure 2b-e) reveal the presence of carbon (75.2 at%), oxygen (7.2 at%), fluorine (17.1 at%), and sodium (~0.5 at%). There is a significant difference between this result and the EDX result, since XPS is a more surface-sensitive technique probing only a few nanometers in depth, and is therefore unable to detect the interior of the nanoparticles. Additionally, XPS is highly sensitive to adsorbed moisture, whilst it is difficult to separate oxygen and carbon using the EDX technique. There are several smaller Auger peaks in the wide-scan corresponding to the C KLL, O KLL, F KLL and Na KLL. The sodium content is very low, as most of the NaF is encapsulated within the carbon shell (as observed in EDX mapping) and therefore cannot be detected by XPS. These XPS results suggest that the composition of the fluorinated carbon is approximately C_4F.

The C1s signal is shown in Figure 2b. It can be deconvoluted into carbon-carbon bonds at 284.5 eV, carbon-oxygen bonds at 285.6 eV, semi-ionic CF / epoxy groups at 286.6 eV, covalent CF at 289.6 eV. There are various small peaks at higher energy which may correspond to small proportions of CF_2 at 291.5 eV, or CF_3 at 294.0 eV, or C1s shake-up. The F 1s spectrum (Figure. 3b) is centered at 688.3 eV, and is largely attributed to a single peak corresponding to covalent CF bonds. There are no significant signals at 685.6, 684.0, or 684.5 eV corresponding to semi-ionic CF, ionic CF or NaF, respectively,[56] suggesting that the majority of F atoms in this material are covalently bonded to carbon. The O1s spectrum is deconvoluted into four main peaks at: 530.0 eV (C=O /NaO), 531.4 eV (C-O), 532.3 eV (O-H / NaOH), and 533.5 eV (adsorbed H_2O). The Na 1s signal (Figure 2e) is deconvoluted into NaO (1073.3 eV) and NaF (1071.3 eV) signals.

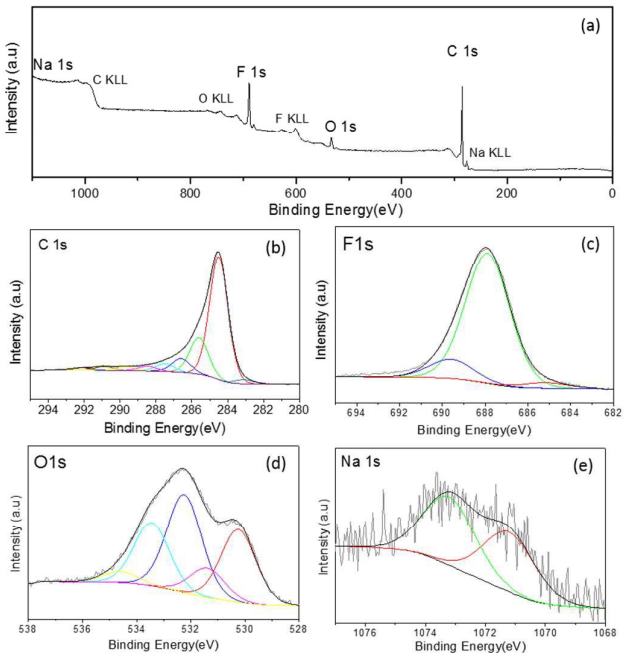

Fig. 2 XPS spectra of the fluorinated carbon nanoparticles. (a) Wide-scan spectrum. High-resolution spectra of the (b) C 1s, (c) F 1s, (d) O 1s, and (e) Na 1s regions.

Raman Spectroscopy

Raman spectroscopy was used to probe the carbon structure. Figure 3a shows the Raman spectra of fluorinated carbon, carbon black, and the unfluorinated ethanol-derived carbon. The Raman peaks observed here are associated only with

vibrational modes in the carbon structure. The energy of the laser is below that of the energy gap of graphite fluoride and therefore Raman signals are not activated by fluorine inclusion.[20] The peak at 1344 cm^{-1} is assigned to the D band of the sp^2 bonded carbon (corresponding to the breathing mode of sp^2 aromatic rings), while the peak at 1591 cm^{-1} is known as the G band of the sp^2 bonded carbon (corresponding to the primary in-plane vibrational mode).[57] The ratio in intensity of the two peaks, I_D/I_G, for fluorinated carbon (1.3) is higher than that of carbon black (1.0) and the ethanol-derived carbon (1.1), indicating that the fluorinated carbon nanoparticles are more defective at the atomic scale,[58] probably due to disruption of the sp^2 carbon network by the covalently bonded fluorine atoms.

X-Ray Diffraction and Selected Area Electron Diffraction

Both the fluorinated and unfluorinated carbons were characterized using XRD (Figure 3b). In the unfluorinated sample, only bands in the spectrum corresponding to broad 002 (~0.40 nm lattice spacing) and 100 (~0.20 nm) crystal planes were observed, suggesting that the material is highly defective, with little long-range order. The spectrum of the fluorinated nanoparticles displays similar signals corresponding to carbon 002 and 100. However several different diffraction features are overlaid with this defective carbon signal. A sharp double peak at around 26˚ (0.34 nm spacing) suggests the presence of some highly crystalline carbon in the fluorinated sample. The peaks at 18˚ (0.50 nm), 42 ˚ (0.20 nm), 39 ˚ (0.23 nm), and 56 ˚ (0.16 nm) correspond to CF_x (002),[14,16] CF_x (100) [15] (confirming that fluorination of the carbon was successful), and NaF, respectively, in agreement with the EDX and XPS results.

The XRD spectrum is averaged over a relatively large area. In order to determine if the crystalline phases observed in the XRD spectra are representative of the nanoparticles or localized in impurities, selected area electron diffraction (SAED) was performed (not shown). This revealed that the individual nanoparticles are generally amorphous, with only diffuse ring-like diffraction patterns. The more crystalline phases are attributed to localized agglomerations of larger carbon particles, in which more fine-structure was observed in the SAED diffraction patterns.

Surface Area and Porosity

The specific surface area and porosity of the materials was investigated using BET nitrogen adsorption. The measured specific surface area is as low as 29 m^2/g, about an order of magnitude lower than that of Vulcan (239 m^2/g), and much lower than the unfluorinated ethanol-derived carbon (>1000 m^2/g). This may be due in part to the large nanoparticle size of the fluorinated carbon compared with carbon black, and the presence of relatively dense NaF inside the hollow shells. Additionally, fluorination is known to reduce micropore volume.[5]

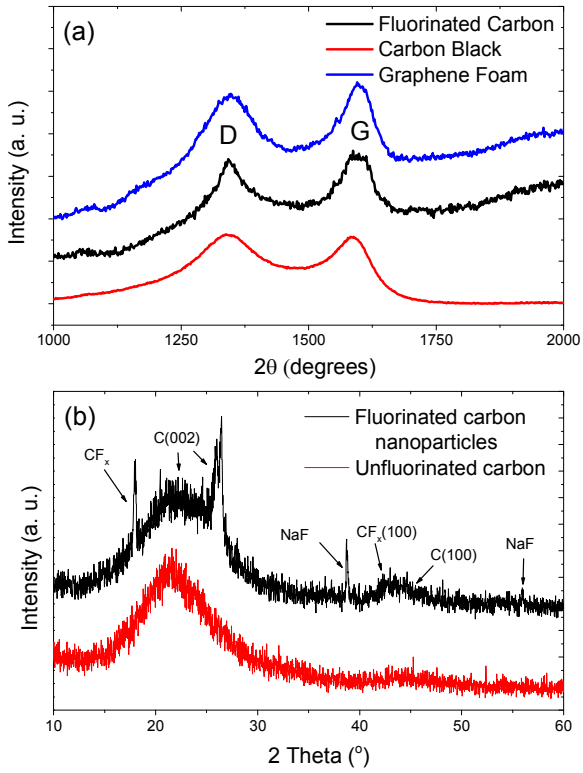

Fig. 3 (a) Raman spectra for the fluorinated nanoparticles, carbon black, and ethanol-derived carbon foam. (b) XRD spectra for the fluorinated nanoparticles and unfluorinated ethanol-derived carbon.

Thermogravimetric Analysis (TGA)

The thermal stability of the hollow fluorinated carbon nanoparticles was investigated by TGA and DTA under air and nitrogen atmosphere (Figure 4). In air, the material is relatively stable up to around 400 ˚C, where the material decomposes exothermically. In nitrogen it is stable up to around 450 ˚C, where decomposition occurs endothermically. In comparison, the unfluorinated analogue derived from sodium ethoxide decomposes at around 250 ˚C in both air and nitrogen. This suggests that fluorination by this method results in increased thermal stability, as commonly observed for fluorinated materials.[59,60] In addition, a significant mass loss is observed at around 100 ˚C in the unfluorinated carbon, suggesting significant adsorption of moisture from the air. In the fluorinated carbon no such peak is observed, suggesting very weak interaction with water.

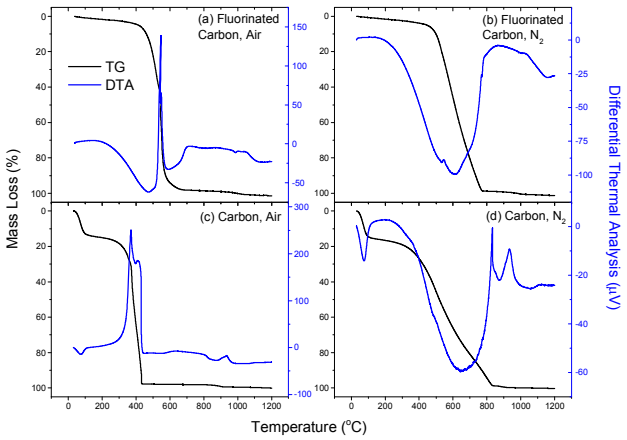

Fig. 4 Thermogravimetric analysis (TGA) and differential thermal analysis (DTA) of fluorinated carbon nanoparticles in (a) air and (b) nitrogen; and unfluorinated carbon in (c) air and (d) nitrogen.

Superhydrophobicity

Many fluorocarbons are hydrophobic.[5,48,61] Therefore, the interaction of the fluorinated carbon nanoparticles with water was investigated. Initially, the powder was added to deionized water and vigorously shaken. No wetting or dispersion of the sample occurred, and the powder remained floating on the surface of the water, even after several weeks (Figure 5a). Conversely, the powder forms a stable dispersion in ethanol (2.5 mg/ml, Figure 5b), allowing solution processing of this product by printing, spraying, or filtration onto various substrates. The ink was vacuum filtered onto: filter paper (Kiriyama, Japan); nylon; and cotton (Figure 5c-e). The ink was also sprayed directly onto silicon (Figure 5f). All of these surfaces were rendered superhydrophobic after treatment with the fluorinated nanoparticles.

The hydrophobicity was quantitatively assessed on PTFE membranes through contact angle measurements, using a sessile drop method. The water contact angle was measured to be 168°, which is significantly high, and confirms the superhydrophobic nature of this material (Figure 5g). However, the interaction between the nanoparticles and the substrate is weak, causing the nanoparticles to easily become detached. We are currently working to minimize this effect and this will be the subject of future publications. The interaction with n-hexadecane was also investigated, and the contact angle was 0°, showing that the nanoparticles are oleophilic, opening up potential applications in e.g. oil separation from water.[49]

In comparison, the contact angles for the non-fluorinated, ethanol-derived carbon was 0° for both water and n-hexadecane, displaying both hydrophilic and oleophilic properties, and confirming that fluorination has a significant impact on the surface properties of the resulting carbon.

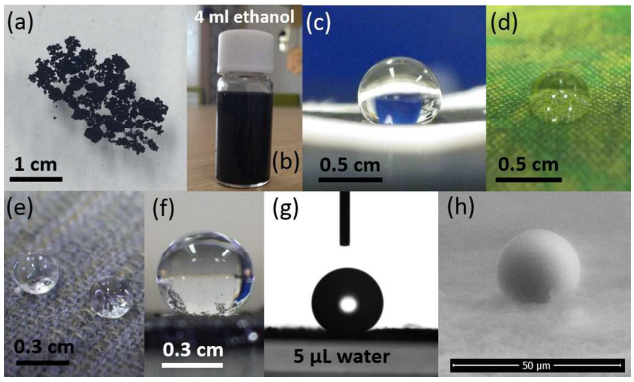

Fig. 5 Photographs of fluorinated carbon nanoparticle powder; (a) floating on water after agitation, and (b) dispersed in ethanol. Printed onto (c) filter paper; (d) nylon; (e) cotton; and (f) sprayed onto silicon. (g) Micrograph of a water droplet on a fluorinated carbon nanoparticle-coated Millipore membrane. (h) Environmental SEM image of a water droplet on a layer of fluorinated nanoparticles.

Conclusions

Fluorinated carbon nanoparticles were synthesized at the gram scale by exothermic reaction between a fluorinated alcohol and sodium metal. The nanoparticles have a hollow-shell morphology and a size of around 50 to 100 nm, and are stable up to around 400 °C in air. The fluorine content was 17.1 at% measured by XPS, comprising mainly covalent CF bonds. After dispersion in ethanol, the nanoparticles were deposited onto a variety of hydrophilic surfaces, rendering them superhydrophobic. This is a new scalable method for the bottom-up fluorination of carbon powders, which could be applied in the mass production of superhydrophobic inks and paints, with potential applications in e.g. waterproofing, de-icing, self-cleaning surfaces, water management in electrochemical devices, and removing oil contamination from water.

Acknowledgements

The authors gratefully acknowledge the support of the International Institute for Carbon Neutral Energy Research (WPI-I2CNER), sponsored by the World Premier International Research Center Initiative (WPI), MEXT, Japan; the International Research Center for Hydrogen Energy, Kyushu University. This work was partially supported by the Core Research for Evolutional Science and Technology (CREST) program from the Japan Science and Technology Agency (JST).

References

1 K. Guérin, M. Dubois, A. Houdayer, A. Hamwi, *J. Fluor. Chem*. 2012, **134**, 11.
2 K. Ueno, N. Watanabe, T. Nakajima, *J. Fluor. Chem.* 1982, **19**, 323.
3 Y. Kita, N. Watanabe, Y. Fujii, *J. Am. Chem. Soc.* 1979, **101**, 3832.

4 G. Nansé, E. Papirer, P. Fioux, F. Moguet, A. Tressaud, *Carbon* N. Y. 1997, **35**, 175.
5 G. Li, K. Kaneko, S. Ozeki, F. Okino, H. Touhara, *Langmuir* 1995, **11**, 716.
6 C.-T. Hsieh, J.-M. Chen, Y.-H. Huang, R.-R. Kuo, C.-T. Li, H.-C. Shih, T.-S. Lin, C.-F. Wu, *J. Vac. Sci. Technol. B* 2006, **24**, 113.
7 E. Disa, K. Guérin, M. Dubois, N. Nomède-Martyr, F. Jestin, A. Hamwi, C. Soubeyrand, M. Manteghetti, *Carbon* N. Y. 2013, **55**, 23.
8 E. Disa, M. Dubois, K. Guérin, H. Kharbache, F. Masin, A. Hamwi, *Carbon* 2011, **49**, 4801.
9 W. Zhang, L. Spinelle, M. Dubois, K. Guérin, H. Kharbache, F. Masin, A. P. Kharitonov, A. Hamwi, J. Brunet, C. Varenne, A. Pauly, P. Thomas, D. Himmel, J. L. Mansot, *J. Fluor. Chem.* 2010, **131**, 676.
10 E. T. Mickelson, C. B. Huffman, A. G. Rinzler, R. E. Smalley, R. H. Hauge, J. L. Margrave, *Chem. Phys. Lett.* 1998, **296**, 188.
11 K. H. An, J. G. Heo, K. G. Jeon, D. J. Bae, C. Jo, C. W. Yang, C.-Y. Park, Y. H. Lee, Y. S. Lee, Y. S. Chung, *Appl. Phys. Lett.* 2002, **80**, 4235.
12 K. Kudin, H. Bettinger, G. Scuseria, *Phys. Rev. B* 2001, **63**, 045413.
13 T. Hayashi, M. Terrones, C. Scheu, Y. A. Kim, M. Rühle, T. Nakajima, M. Endo, *Nano Lett*. 2002, **2**, 491.
14 B. Shen, J. Chen, X. Yan, Q. Xue, *RSC Adv*. 2012, **2**, 6761.
15 Y. M. Shulga, T.-C. Tien, C.-C. Huang, S.-C. Lo, V. E. Muradyan, N. V. Polyakova, Y.-C. Ling, R. O. Loutfy, A. P. Moravsky, *J. Electron Spectros. Relat. Phenomena* 2007, **160**, 22.
16 A. Hamwi, H. Alvergnat, S. Bonnamy, F. Béguin, *Carbon* N. Y. 1997, **35**, 723.
17 J. T. Robinson, J. S. Burgess, C. E. Junkermeier, S. C. Badescu, T. L. Reinecke, F. K. Perkins, M. K. Zalalutdniov, J. W. Baldwin, J. C. Culbertson, P. E. Sheehan, E. S. Snow, *Nano Lett*. 2010, **10**, 3001.
18 R. Stine, W.-K. Lee, K. E. Whitener, J. T. Robinson, P. E. Sheehan, *Nano Lett*. 2013, **13**, 4311.
19 B. Wang, J. Wang, J. Zhu, *ACS Nano* 2014, **8**, 1862.
20 R. R. Nair, W. Ren, R. Jalil, I. Riaz, V. G. Kravets, L. Britnell, P. Blake, F. Schedin, A. S. Mayorov, S. Yuan, M. I. Katsnelson, H.-M. Cheng, W. Strupinski, L. G. Bulusheva, A. V Okotrub, I. V Grigorieva, A. N. Grigorenko, K. S. Novoselov, A. K. Geim, *Small* 2010, **6**, 2877.
21 X. Hong, S.-H. Cheng, C. Herding, J. Zhu, *Phys. Rev. B* 2011, **83**, 085410.
22 F. Withers, M. Dubois, A. K. Savchenko, *Phys. Rev. B* 2010, **82**, 073403.
23 Y. C. Hong, H. S. Uhm, *Appl. Phys. Lett*. 2006, **88**, 244101.
24 R. Zbořil, F. Karlický, A. B. Bourlinos, T. A. Steriotis, A. K. Stubos, V. Georgakilas, K. Šafářová, D. Jančík, C. Trapalis, M. Otyepka, *Small* 2010, **6**, 2885.
25 Y. Lin, G. J. Ehlert, C. Bukowsky, H. A. Sodano, *ACS Appl. Mater. Interfaces* 2011, **3**, 2200.
26 W. Zhang, K. Guérin, M. Dubois, Z. El Fawal, D. A. Ivanov, L. Vidal, A. Hamwi, *Carbon* 2008, **46**, 1010.
27 X. Yu, K. Lin, K. Qiu, H. Cai, X. Li, J. Liu, N. Pan, S. Fu, Y. Luo, X. Wang, *Carbon* 2012, **50**, 4512.
28 W. Navarrini, C. L. Bianchi, L. Magagnin, L. Nobili, G. Carignano, P. Metrangolo, G. Resnati, M. Sansotera, *Diam. Relat. Mater.* 2010, **19**, 336.
29 K. K. S. Lau, J. Bico, K. B. K. Teo, M. Chhowalla, G. A. J. Amaratunga, W. I. Milne, G. H. McKinley, K. K. Gleason, *Nano Lett.* 2003, **3**, 1701.
30 K.-J. Jeon, Z. Lee, E. Pollak, L. Moreschini, A. Bostwick, C.-M. Park, R. Mendelsberg, V. Radmilovic, R. Kostecki, T. J. Richardson, E. Rotenberg, *ACS Nano* 2011, **5**, 1042.
31 F. Karlický, K. Kumara Ramanatha Datta, M. Otyepka, R. Zbořil, *ACS Nano* 2013, **7**, 6434.
32 S. H. Lai, K. P. Huang, Y. M. Pan, Y. L. Chen, L. H. Chan, P. Lin, H. C. Shih, *Chem. Phys. Lett.* 2003, **382**, 567.
33 K. Honda, M. Morita, O. Sakata, S. Sasaki, A. Takahara, *Macromolecules* 2010, **43**, 454.
34 K. Honda, M. Morita, A. Takahara, *Soft Matter* 2008, **4**, 1400.
35 K. Honda, M. Morita, H. Masunaga, S. Sasaki, M. Takata, A. Takahara, *Soft Matter* 2010, **6**, 870.
36 R. E. Johnson, R. H. Dettre, *J. Phys. Chem.* 1964, **68**, 1744.
37 M. Chinappi, F. Gala, G. Zollo, C. M. Casciola, *Philos. Trans. A. Math. Phys. Eng. Sci.* 2011, **369**, 2537.
38 C. W. Extrand, *Langmuir* 2002, **18**, 7991.
39 C. W. Extrand, *Langmuir* 2004, **20**, 5013.
40 C. W. Extrand, Y. Kumagai, *J. Colloid Interface Sci.* 1997, **191**, 378.
41 L. Gao, T. J. McCarthy, *Langmuir* 2006, **22**, 6234.
42 L. Gao, T. J. McCarthy, *Langmuir* 2006, **22**, 2966.
43 N. Nomède-Martyr, E. Disa, K. Guérin, M. Dubois, L. Frezet, A. Hamwi, *J. Colloid Interface Sci.* 2013, **400**, 11.
44 C. NEINHUIS, *Ann. Bot.* 1997, **79**, 667.
45 M. Hikita, K. Tanaka, T. Nakamura, T. Kajiyama, A. Takahara, *Langmuir* 2005, **21**, 7299.
46 W. Ma, H. Wu, Y. Higaki, H. Otsuka, A. Takahara, *Chem. Commun. (Camb).* 2012, **48**, 6824.
47 W. Ma, Y. Higaki, H. Otsuka, A. Takahara, *Chem. Commun. (Camb).* 2013, **49**, 597.
48 L.-Y. and P. Meng, Soo-Jin, *"CARBON LETT,"* 2014.
49 Y. Wang, Y. Shi, L. Pan, M. Yang, L. Peng, S. Zong, Y. Shi, G. Yu, *Nano Lett.* 2014, DOI 10.1021/nl5019782.
50 H. Nakajima, T. Konomi, T. Kitahara, *J. Power Sources* 2007, **171**, 457.
51 G. Kostov, M. Holan, B. Ameduri, M. H. Hung, *Macromolecules* 2012, **45**, 7375.
52 S. M. Lyth, Y. Nabae, N. M. Islam, T. Hayakawa, S. Kuroki, M. Kakimoto, S. Miyata, *eJournal of Solid State Science and Technology*, 2012, **10**, 29.
53 S. M. Lyth, H. Shao, J. Liu, K. Sasaki, *Int. J. Hydrogen Energy* 2014, **39**, 376.
54 J. Liu, D. Takeshi, D. Orejon, K. Sasaki, S. M. Lyth, *J. Electrochem. Soc.* 2014, **161**, F544.
55 A. Tressaud, F. Moguet, S. Flandrois, M. Chambon, C. Guimon, G. Nanse, E. Papirer, V. Gupta, O. P. Bahl, *J. Phys. Chem. Solids* 1996, **57**, 745.
56 "NIST X-ray Photoelectron Spectroscopy Database, Version 4.1 (National Institute of Standards and Technology, Gaithersburg, 2012); http://srdata.nist.gov/xps/," can be found under http://srdata.nist.gov/xps/faq.aspx, n.d.
57 J. Liu, D. Takeshi, K. Sasaki, S. M. Lyth, *J. Electrochem. Soc.* 2014, **161**, F838.
58 A. C. Ferrari, J. C. Meyer, V. Scardaci, C. Casiraghi, M. Lazzeri, F. Mauri, S. Piscanec, D. Jiang, K. S. Novoselov, S. Roth, A. K. Geim, *Phys. Rev. Lett.* 2006, **97**, 187401.
59 B. Ameduri, *Chem. Rev* 2009, **109**, 6632.
60 F. Boschet, B. Ameduri, *Chem. Rev*. 2014, **114**, 927.
61 H. Touhara, F. Okino, *Carbon* N. Y. 2000, **38**, 241.